Single- and Two-Frequency Sub-THz Waveguide Notch Filters With Rejection Frequencies Within and Beyond the Passband

Dietmar Wagner [ID], *Senior Member, IEEE*, Walter Kasparek, Fritz Leuterer, Francesco Monaco, Burkhard Plaum, Tobias Ruess, Harald Schütz, Jörg Stober [ID], and Manfred Thumm [ID], *Life Fellow, IEEE*

Abstract—Notch filters are a key component in millimeter-wave plasma diagnostics systems for magnetically confined fusion plasmas. They are required to protect sensitive millimeter-wave receivers from stray radiation of electron cyclotron heating systems. These heating systems employ gyrotrons that emit strong millimeter-wave radiation (90 dBm) in one or, in the case of modern step-tunable gyrotrons, several narrowband frequency lines. In this article, we describe the design and performance of notch filters based on waveguide technology, operating in the F-band (90–140 GHz), that reject one or two selectable frequencies in the passband. We also present the solution for a filter where the rejected frequencies are outside of the passband of the plasma diagnostics. This is demonstrated for a filter operating in the W-band (75–110 GHz). To fully protect the diagnostic systems, typical stopbands with not less than 60-dB rejection and at least 500-MHz width are required.

Index Terms—Electron cyclotron resonance heating, notch filter, rectangular waveguide, step-tunable gyrotron, stray radiation.

I. INTRODUCTION

MODERN electron cyclotron resonance heating (ECRH) systems in thermonuclear fusion plasma experiments employ megawatt-class gyrotrons, which operate at frequencies in the millimeter-wave range. In recent years, also gyrotrons were installed, which can be tuned to a second frequency corresponding to another reflection minimum of their single-disk CVD diamond vacuum window [1], [2], [3], [4]. Such gyrotrons became very attractive since they allow for more flexibility with respect to the applied magnetic field in the magnetic confinement fusion devices [5]. Sensitive millimeter-wave diagnostic systems, which have to record signal levels in the microwatt range, need protection against

ECRH stray radiation [6], [7]. The local power densities of this stray radiation can amount to several tens of kW/m^2 [8]. However, new dual-frequency ECRH systems [9] impose a severe problem for sensitive millimeter-wave diagnostics operating in the same frequency band since now more than one frequency needs to be rejected. Notch filters with two stopbands are required, which have to provide a certain width in order to cope for the frequency chirp at the beginning of a gyrotron pulse [10]. In addition, if the ECRH system employs more than one gyrotron, their individual resonance frequencies can be different as well. Typical specifications of high-power gyrotrons allow for a frequency drift around the center frequencies, which in the case of the ASDEX Upgrade gyrotrons are 105 and 140 GHz ± 250 MHz. Therefore, the typical required width of the stopbands must be in the range of 0.5–1.0 GHz. Due to the potentially high stray radiation levels, the rejection of the stopbands must be better than 60 dB. The requirement of both very deep (>60 dB) and wide (>500 MHz) stopbands is very difficult to meet at such high frequencies with available filter technology, such as fundamental waveguide filters with a large number of coupled cylindrical cavities, quasi-optical resonance filters, or molecular absorption gases [6]. Filters based on Bragg reflection structures in cylindrical waveguides [11], [12] could meet the specifications but turned out to be very expensive in manufacturing due to the excessive precision required for these very long waveguide structures. A similar technique in rectangular cross section was also successfully applied in low-pass filters for space applications at somewhat lower frequencies (10–40 GHz) [13]. Bandpass filters at Ku-band with only inductive and capacitive stubs in a rectangular waveguide were presented in [14]. A compact two-frequency filter for 105/140 GHz in the D-band with five cavities was presented in [15]. Similar notch filters are required in lower frequency bands of broadband millimeter-wave diagnostic systems such as reflectometry or electron cyclotron emission (ECE), where, however, low insertion loss, typically 0–2 dB [7], over their full waveguide frequency band has to be maintained. In Section II, we describe our approach to the filter design based on mode matching. In Section III, we present notch filters for F-band waveguides (90–140 GHz) with a single stopband at 140 GHz and also a version with two stopbands at 105 and 140 GHz, both with low insertion loss and

improved passband characteristics in comparison with the two-frequency filter described in [15]. Gyrotron frequencies above the waveguide band in which the diagnostic system operates are a challenge for the design of standard coupled cavity filters, where cavities are either capacitively or inductively coupled to a standard monomode waveguide. Above the passband, the connecting waveguide is oversized, i.e., higher order modes besides the fundamental TE_{10} mode can propagate and vary the phasing between and the coupling to the cavities. In our case, cavities are used in transmission. In addition, when the gyrotron frequency is above the frequency band of the diagnostic system, the waveguide is oversized at the stopband frequencies, and thereby, also higher order modes need to be considered and either be rejected or suppressed. In Section IV, we present a solution for such a case in the W-band (75–110 GHz). Section V shortly summarizes the results.

II. SIMULATION METHOD

Coupled waveguide resonators are realized using symmetric steps in the width of the rectangular waveguide. Therefore, incoming $TE_{m,0}$ modes can only couple to $TE_{2m+n,0}$ modes with $n = 1, 2, 3, \ldots$, for symmetry reasons. This significantly limits the mode spectrum in the filter [16]. To accurately model the filters, the mode matching method [16], [17] is applied considering both propagating plus several additional evanescent modes. This technique takes advantage of the knowledge of the eigenmodes of rectangular waveguides and of the related analytical coupling factors for the step-type coupling. In comparison to 3-D full-field solvers, only discretization along the waveguide axis is required. Cascading several waveguide steps allows for fast and accurate calculation of the filter characteristic. Two-dimensional field plots were done by superposition of the modal fields along the waveguide considering both amplitude and phase of the calculated modal distribution along the filter [15]. The frequency characteristics are given by the transmitted power, which corresponds to the forward transmission S-parameter S_{21} of the propagating modes at the input and output of the filters, as a function of frequency.

III. F-BAND SINGLE- AND TWO-FREQUENCY NOTCH FILTER

For an ECE diagnostic at ASDEX Upgrade, notch filters are required for both 105 and 140 GHz. Both frequencies are within the transmission band of the standard WR08 waveguide.

The cutoff frequency of the fundamental TE_{10} mode in the WR08 waveguide is 73.768 GHz. The cutoff frequency of the first higher order modes (TE_{01} and TE_{20}) is 147.536 GHz. This means that, at both gyrotron frequencies, the WR08 waveguide between the cavities can only propagate the fundamental TE_{10} mode. The calculated minima of the forward transmission coefficient S_{21} for a single rectangular cavity at both frequencies as a function of the width a_r and the length l_r are given in Fig. 1. Two propagating plus additionally six evanescent modes were considered for the calculations. There are many solutions for a single-frequency filter, for example, those ones
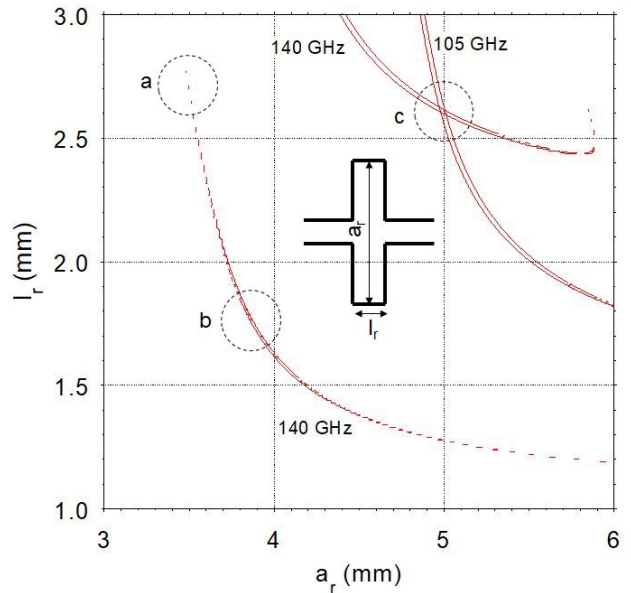

Fig. 1. Calculated S_{21} of an incident TE_{10} mode in a WR08 waveguide as a function of width a_r and length l_r of a single waveguide cavity. The red lines mark the domains where the transmitted power is below -23 dB. The dashed circles show solutions for (a) and (b) single-frequency 140-GHz filter and (c) two-frequency (105/140 GHz) filter.

labeled with (a) and (b) in Fig. 1. However, if the cavity is supposed to reject both frequencies, there is only one solution where the contour lines of the reflection minima for 105 and 140 GHz cross, labeled (c) in Fig. 1 [15].

A. F-Band Single-Frequency Notch Filter

For the single-frequency notch filter for F-band (90–140 GHz) with only one stopband at 140 GHz, there exists a range of cavity dimensions where the resonant mode is dominantly TE_{30}. The forward transmission coefficient S_{21} of two different single cavities with dimensions indicated by the dashed circles (a) and (b) in Fig. 1 was calculated by mode matching. The cavity with the larger width [Fig. 2(b)] causes a wider notch compared to the smaller cavity [Fig. 2(a)], which also exhibits steeper slopes at the stopband. The steepness of the slopes and the notch depth can be further increased by increasing the number of cavities [15]. A filter with five cavities with geometry [Fig. 2(a)] was built in split block technology and tested. The geometry of this filter is shown in Fig. 3. A comparison between calculated and measured transmission characteristics (see Fig. 4) shows an excellent agreement. Since the F-band modules of the VNA used for this measurement were limited to a maximum frequency of approximately 141 GHz, we added a second measurement in D-band, also employing WR08-WR06 transitions. Fig. 5(a) shows the calculated normalized mode distribution along the filter at 140 GHz. The two-dimensional intensity distribution ($|E|^2$) in the plane of the width of the waveguide in Fig. 5(b) was calculated by superposition of the modal fields.

B. F-Band Two-Frequency Notch Filter

The geometry for a two-frequency filter with two stopbands at 105 and 140 GHz in the F-band (90–140 GHz) is indicated
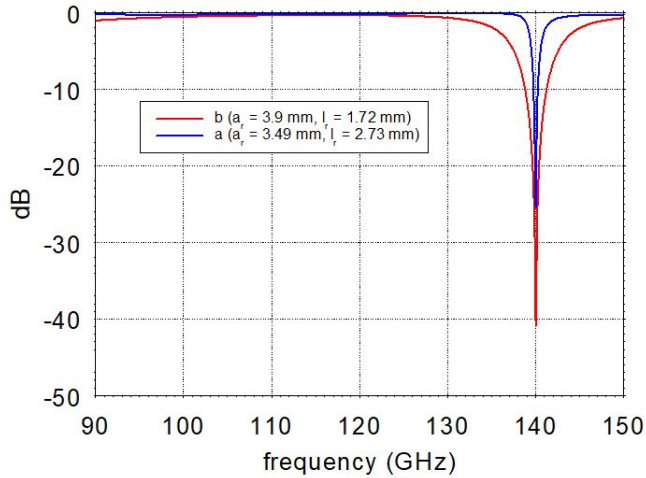
Fig. 2. Calculated S_{21} of a single cavity filter for 140 GHz with dimensions: (a) $a_r = 3.49$ mm, $l_r = 2.73$ mm and (b) $a_r = 3.90$ mm and $l_r = 1.72$ mm.
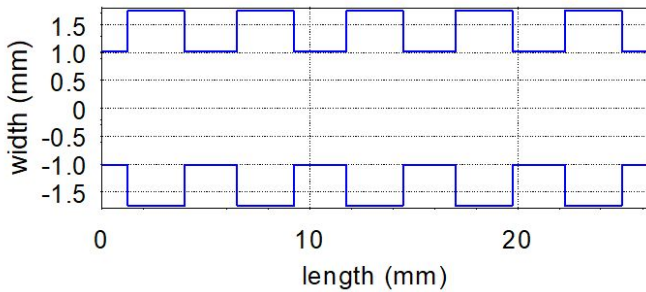

Fig. 3. Geometry (rectangular waveguide width) of the five-cavity 140-GHz filter for F-band. The waveguide has a constant height of 1.016 mm.
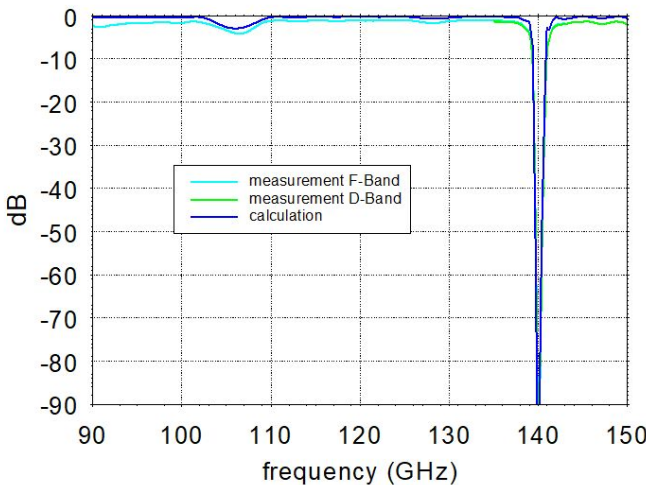

Fig. 4. Comparison between measured and calculated frequency characteristics (S_{21}) of the five-cavity 140 GHz notch filter for the F-band. To show the filter performance above the stopband at 140 GHz, a second measurement with transition to the D-Band is added to the figure.

by the dashed circle in Fig. 1(c). In order to reduce the ripples between the two stopbands at 105 and 140 GHz, we reduced the quality factor of the cavities by applying a
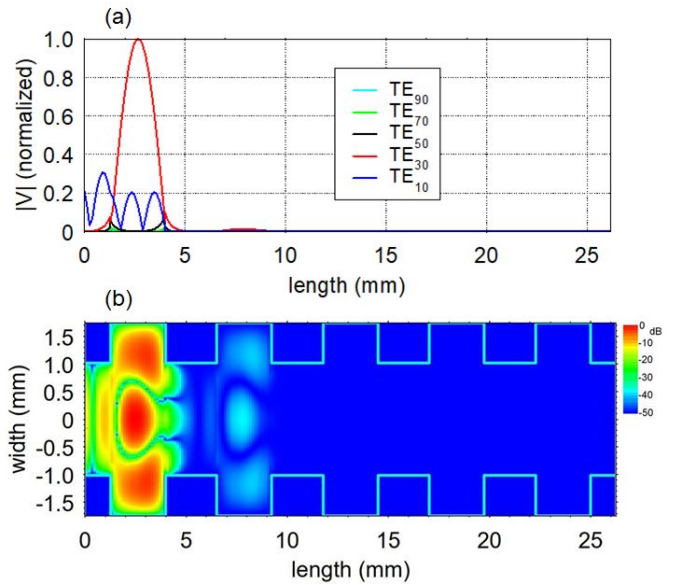

Fig. 5. (a) Normalized mode amplitude distribution and (b) normalized intensity distribution along the five-cavity 140-GHz notch filter for the F-band at $f = 140$ GHz.
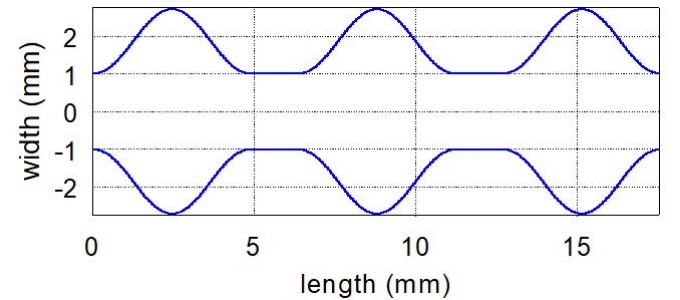

Fig. 6. Geometry of the three-cavity 105-/140-GHz filter for the F-band. The waveguide has a constant height of 1.016 mm.

rounded design [13], [18], [19], [20]. The geometry of the two-frequency notch filter and a photograph of it without the top plate are given in Figs. 6 and 7. To model this geometry with the mode matching technique, we applied a step-ladder approach, representing the sinusoidal contour by a large number of steps in the waveguide width. In this case, the number of steps per cavity is 100. The comparison between calculated and measured frequency characteristics, given in Fig. 8, shows an excellent agreement. The calculated normalized mode and two-dimensional intensity distributions ($|E|^2$) along the filter at the resonances at 105 and 140 GHz are plotted in Figs. 9 and 10, respectively. For comparison, Fig. 11 shows the normalized mode and intensity distribution outside of the cavity resonances at 120 GHz.

IV. W-BAND TWO-FREQUENCY NOTCH FILTER WITH REJECTION FREQUENCIES ABOVE THE PASSBAND

A particular problem arises for millimeter-wave diagnostics that operate in a standard waveguide frequency band below the gyrotron frequencies. Usual coupled cavity filters [6]

Fig. 7.   Three-cavity 105-/140-GHz filter for the F-band, realized in split-block technology.
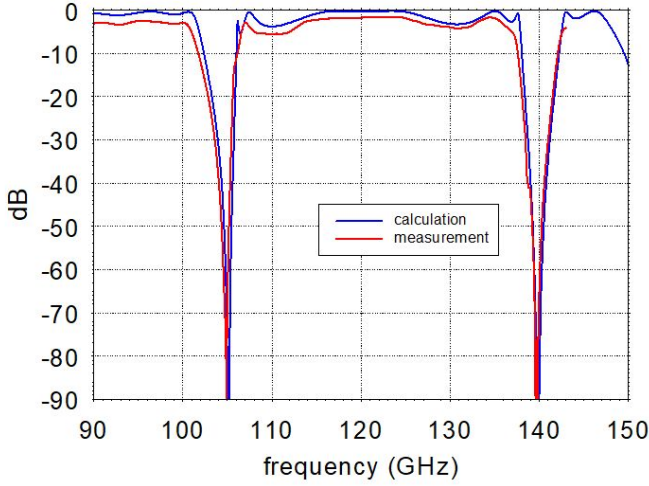

Fig. 8.   Comparison between measured and calculated frequency characteristics (S_{21}) of the three-cavity 105-/140-GHz notch filter for the F-band.
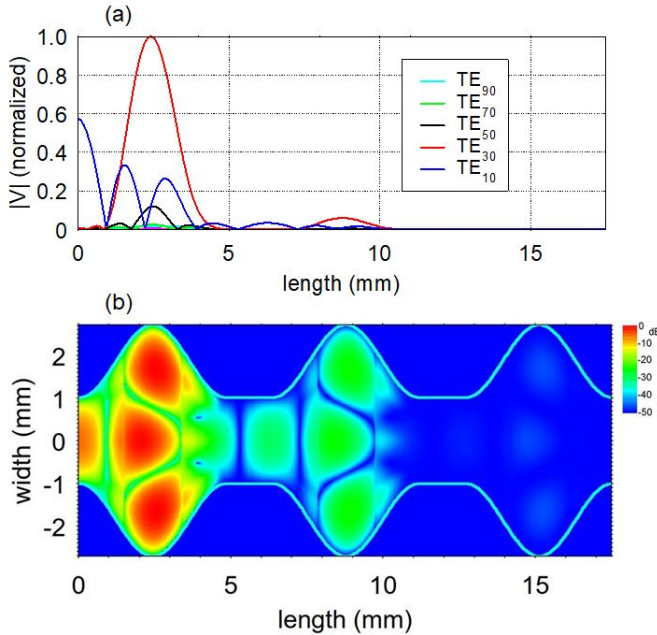

Fig. 9.   (a) Normalized mode amplitudes and (b) intensity distribution along the three-cavity 105-/140-GHz notch filter for the F-band at $f = 105$ GHz.
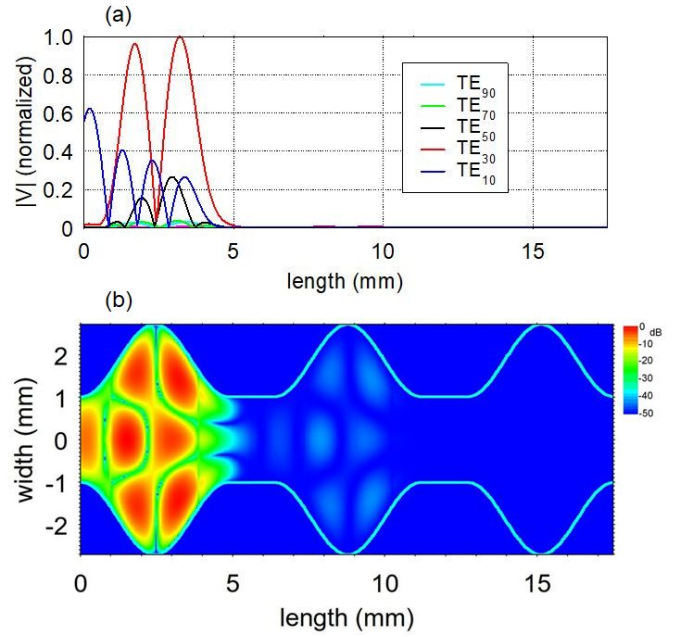

Fig. 10.   (a) Normalized mode amplitudes and (b) intensity distribution along the three-cavity 105-/140-GHz notch filter for the F-band at $f = 140$ GHz.
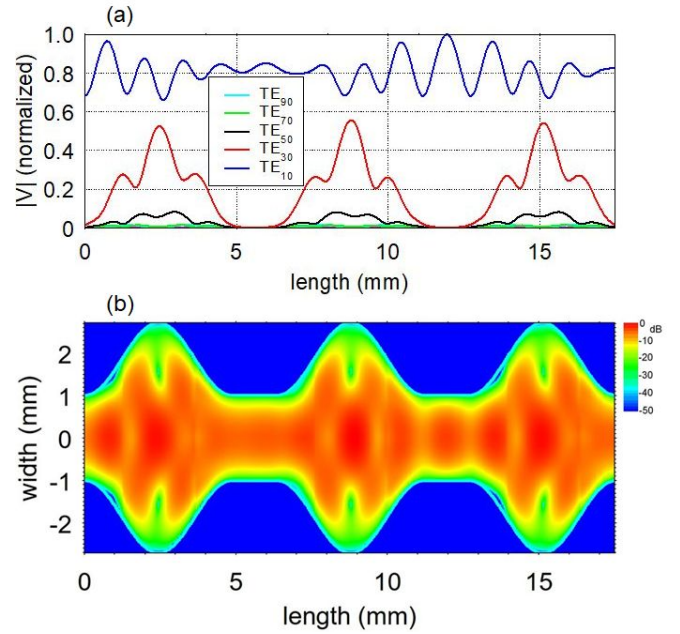

Fig. 11.   (a) Normalized mode amplitudes and (b) intensity distribution along the three-cavity 105-/140-GHz notch filter for the F-band at $f = 120$ GHz.

operate with cavities connected to a fundamental waveguide via capacitive or inductive coupling through holes or slits with dimensions below cutoff. In the WR10 waveguide, the cutoff frequency of the fundamental TE_{10} mode is 59.015 GHz. The cutoff frequency of the first higher order modes (TE_{01} and TE_{20}) is 118.03 GHz. This means that for gyrotron frequencies above 118 GHz, this waveguide is oversized and can therefore support more than one propagating mode.

In our particular case, a dual-frequency notch filter is required to protect a reflectometry system [21] operating in the W-band (75–110 GHz) against stray radiation from the ASDEX Upgrade dual-frequency ECRH system with
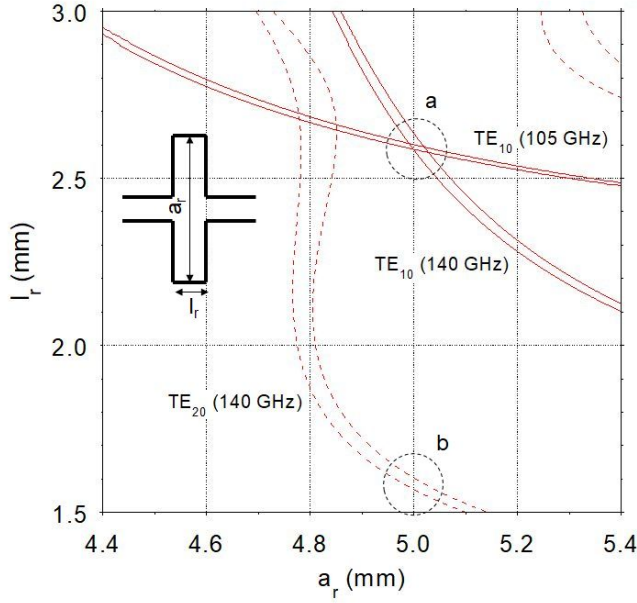
Fig. 12. Calculated minima of S_{21} of the TE_{10} mode at 105 and 140 GHz as a function of width a_r and length l_r of the waveguide cavity (solid lines) and the TE_{20} mode at 140 GHz (dashed lines). The red lines mark the domains where the S_{21} is below -23 dB. The dashed circle (a) marks the dimensions where the minima for both frequencies meet for TE_{10} as input mode. The dashed circle (b) marks the dimensions chosen for the 140-GHz TE_{20} cavities.
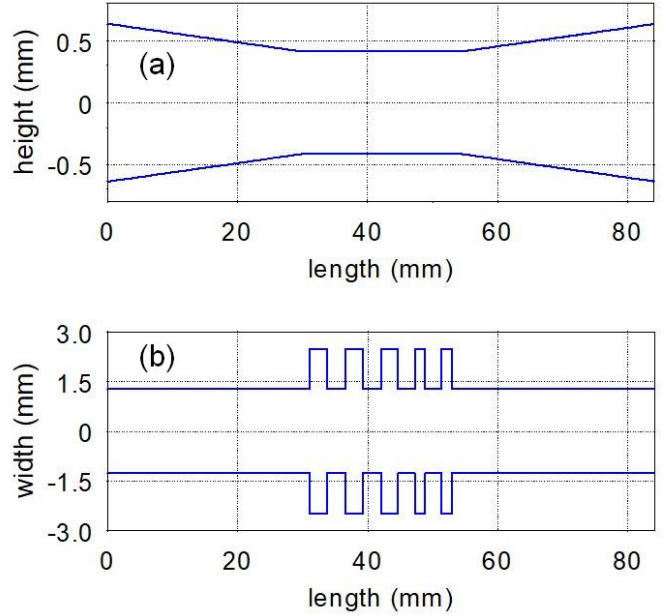

Fig. 13. Contours of the waveguide (a) height and (b) width of the two-frequency notch filter for the W-band. Both input and output flanges of this waveguide match with the WR10 standard.
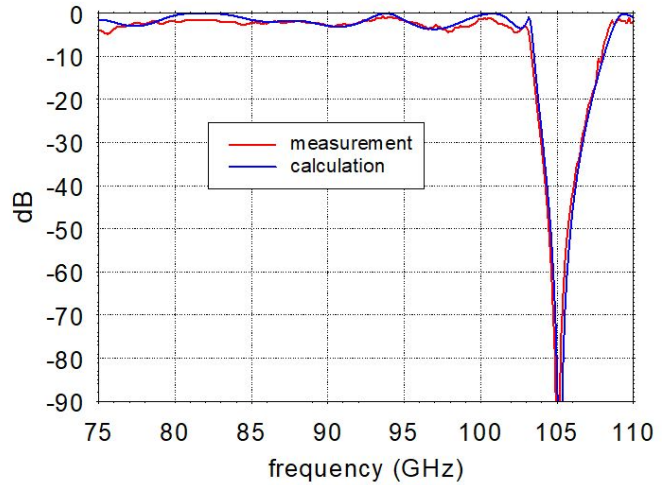

Fig. 14. Comparison of calculated and measured S_{21} of the filter with the geometry given in Fig. 13 in the W-band.

gyrotrons operating at 105 and 140 GHz. The lower gyrotron frequency (105 GHz) is within the W-band, and therefore, the only propagating mode in the WR10 waveguide is the fundamental TE_{10} mode. At 140 GHz, four TE_{mn} modes and one TM_{mn} mode can propagate in a WR10 waveguide (2.54 × 1.27 mm). These are TE_{10}, TE_{20}, TE_{01}, TE_{11}, and TM_{11}. The oversized horn antenna of the reflectometry system can excite all these modes at 140 GHz if connected to a WR10 waveguide. All modes with $n \neq 0$ can be suppressed by tapering of the waveguide height down to a size, which is below half of the free-space wavelength at 140 GHz at the entrance of the filter. Here, the height of a standard rectangular waveguide for D-band, $b = 0.855$ mm, was chosen. This means that between 118.03 and 181.583 GHz, which corresponds to the cutoff frequency of the TE_{01} mode, only two modes, namely, TE_{10} and TE_{20}, can propagate in the waveguide between cavities. This reduces the spectra of propagating modes to just one mode (TE_{10}) at 105 GHz and two modes (TE_{10}, TE_{20}) at 140 GHz. For the two remaining TE_{m0} modes, the same filter technology can be applied as in [15]. Here, we combine a two-frequency (105/140 GHz) filter for the TE_{10} mode with a one-frequency (140 GHz) filter for the TE_{20} mode.

The optimum dimensions of the TE_{10}-mode cavity can be determined by calculating the forward transmission coefficient S_{21} at both 105 and 140 GHz as a function of both the width a_r and the length l_r of a single cavity [15]. Fig. 12 shows the minima of S_{21} at both frequencies, again by the -23 dB lines. The point where both domains cross [dashed circle (a)] gives the correct dimension of the desired cavity for TE_{10} as input mode ($a_r = 5.0$ mm, $l_r = 2.586$ mm). For the TE_{20} mode filter at 140 GHz, we choose a cavity with the

same width ($a_r = 5.0$ mm) but different lengths ($l_r = 1.584$ mm), as marked by the dashed circle (b). To achieve sufficient rejection at 105 and 140 GHz for the TE_{10} mode, the number of cavities chosen is three. The rejection of the TE_{20} mode by these cavities is only 20 dB. Therefore, we added two additional cavities for the TE_{20} mode in order to provide a similar rejection compared to the TE_{10} mode. The geometry of this filter is plotted in Fig. 13. A comparison between measured and calculated frequency characteristics in the W-band (75–110 GHz) shows excellent agreement in the notch and exhibits low insertion loss in the passband (see Fig. 14). The calculated normalized mode distributions and the two-dimensional intensity distribution ($|E|^2$) along the resonators for $f = 105$ GHz are plotted in Fig. 15.
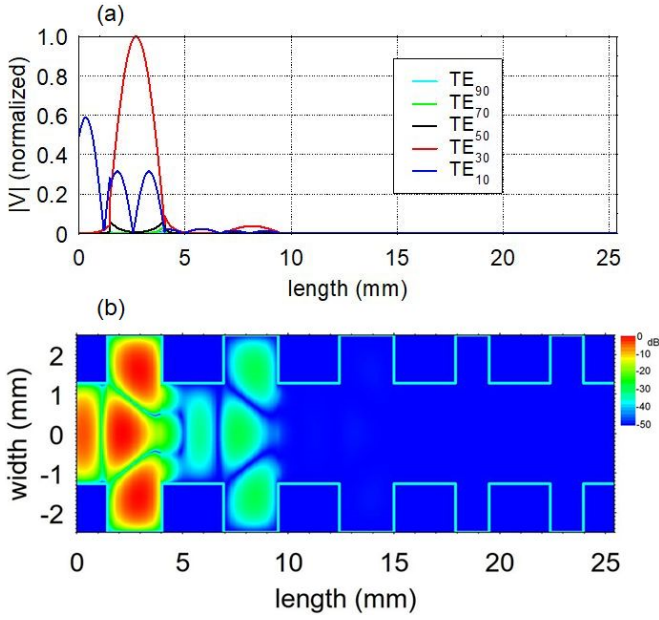
Fig. 15. (a) Normalized mode amplitudes and (b) intensity distribution along the five-cavity 105-/140-GHz notch filter for the W-band at $f = 105$ GHz with TE_{10} as input mode.
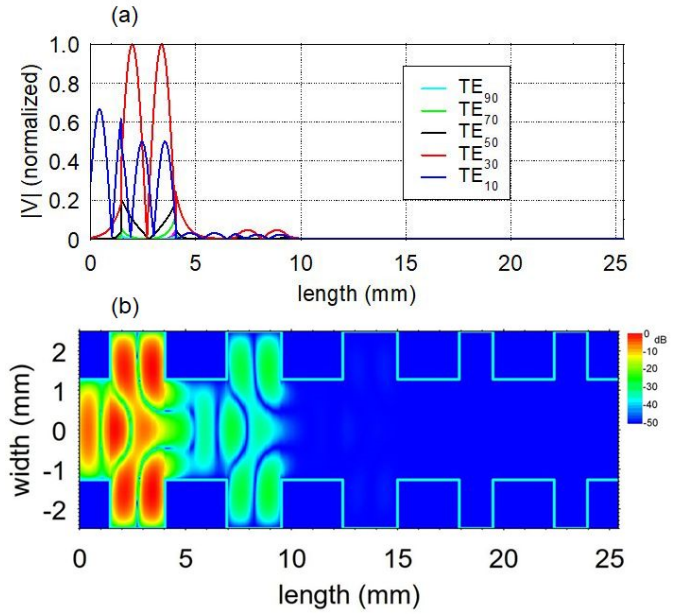

Fig. 17. (a) Normalized mode amplitudes and (b) intensity distribution along the five-cavity 105-/140-GHz notch filter for the W-band at $f = 140$ GHz with TE_{10} as input mode.
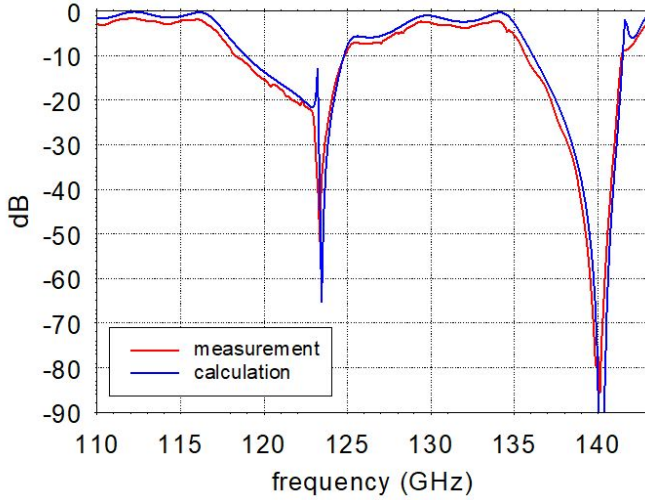

Fig. 16. Comparison between calculated and measured transmission of the filter with the geometry given in Fig. 13 with TE_{10} as input mode for frequencies above the W-band.
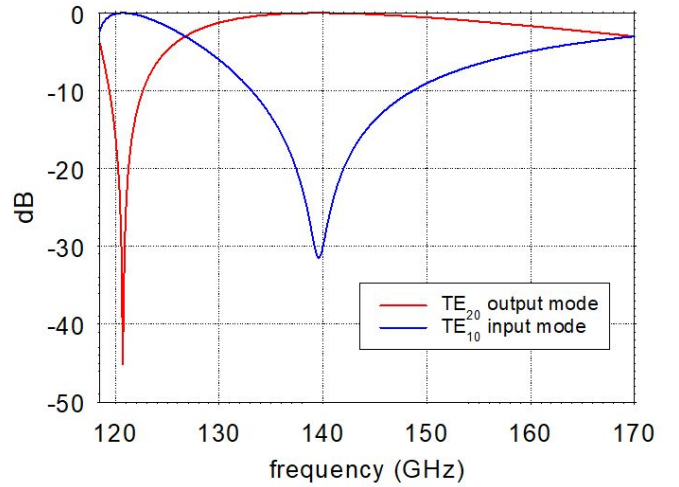

Fig. 18. Calculated mode conversion of the TE_{10}–TE_{20} mode converter. Only at 140-GHz a pure TE_{20} output mode is excited.

The second stopband at 140 GHz lies above the W-band passband (75–110 GHz). Here, the filter needs to reject both propagating modes TE_{10} and TE_{20}. A comparison between calculated and measured forward transmission coefficient S_{21} for TE_{10} as input mode is plotted in Fig. 16. There are additional ripples and resonances in this frequency range besides the notch at 140 GHz, which are due to coupling of the TE_{10} input mode at the two TE_{20} cavities. However, they do not affect the functionality of the filter, since the diagnostic only operates in the W-band and only the rejection of the gyrotron frequency of 140 GHz has to be provided for both propagating modes. The calculated normalized mode and intensity distributions ($|E|^2$) along the filter at 140 GHz with input in the TE_{10} mode are plotted in Fig. 17.

In order to test the W-band two-frequency notch filter also with TE_{20} as input mode, two TE_{10}–TE_{20} mode converters [22] in W-band dimensions were used. The calculated mode conversion as a function of frequency of such a mode converter is plotted in Fig. 18. Only at the notch frequency of 140 GHz, we can realize a pure TE_{20} input mode for the filter. At other frequencies above the cutoff frequency for the TE_{02} mode (118.583 GHz), the input to the filter is inevitably a mixture of TE_{10} and TE_{20} modes. The special setup, which was only used for the measurements with the TE_{20} mode, is shown in Fig. 19. The comparison between the calculated and measured
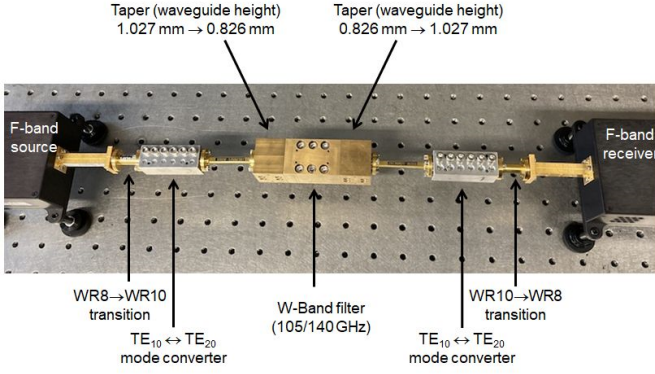
Fig. 19. Measurement setup for the W-band two-frequency (105/140 GHz) notch filter.
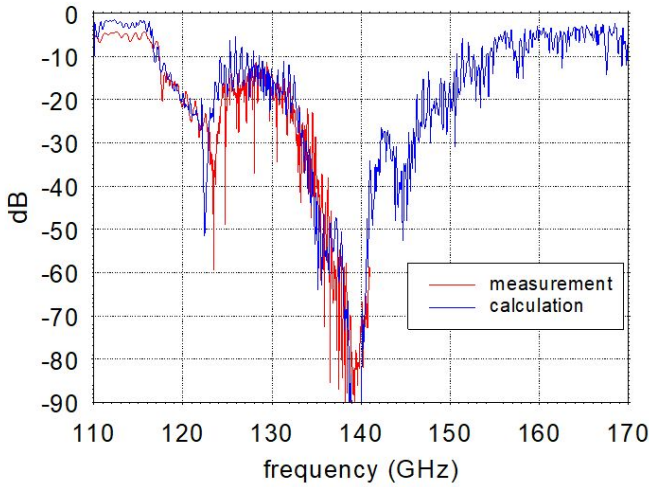

Fig. 20. Comparison between calculated and measured transmission of the filter with the geometry given in Fig. 15 for a TE_{10}/TE_{20} input mode mixture according to Fig. 18.
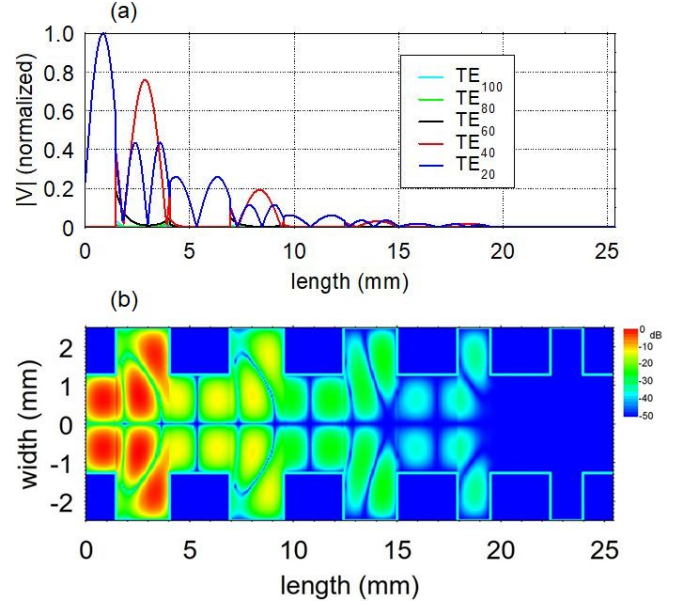

Fig. 21. (a) Normalized mode amplitudes and (b) intensity distribution along the five-cavity 105-/140-GHz notch-filter for the W-band at $f = 140$ GHz for TE_{20} as input mode.

TABLE I

COMPARISON OF THE MEASURED STOPBAND WIDTHS Δf WITH THE VALUES FOR THE FILTERS PUBLISHED IN [6], [17], [18], AND [19]

Filter	Rejected Frequency	Δf at -30 dB	Δf at -60 dB
[6]	110 GHz	184 MHz	-
[17]	70 GHz	280 MHz	-
[18]	68 GHz	1014 MHz	544 MHz
[19]	70 GHz	275 MHz	184 MHz
[19]	170 GHz	1024 MHz	690 MHz
Here, Sc. III. A	140 GHz	1077 MHz	656 MHz
Here, Sc. III. B	105 GHz	1814 MHz	473 MHz
	140 GHz	2523 MHz	631 MHz
Here, Sc. IV	105 GHz	2622 MHz	736 MHz
	140 GHz	2819 MHz	868 MHz

forward transmission coefficients S_{21} with two TE_{10}–TE_{20} mode converters connected to both ends of the notch filter is plotted in Fig. 20. The TE_{20} content in the input mode mixture in this measurement is limited by the efficiency of the mode converter (see Fig. 18). For these tests, we utilized a source and detectors operating in the F-band, and therefore, there are also F- to W-band transitions on both sides. Trapping of the TE_{20} mode between the converters and these transitions causes the standing wave content seen in this measurement (see Fig. 20). This was not the case for the measurements with the TE_{10} as input mode (see Figs. 14 and 16), for which the waveguide transitions are transparent in this frequency range. Nevertheless, our measurements clearly demonstrate a high rejection (∼80 dB) of both modes at 140 GHz and therefore prove the functionality of the notch filter also in the frequency range where the waveguide is oversized and supports two propagating modes (TE_{10} and TE_{20}). The calculated normalized mode distributions and the two-dimensional intensity distribution ($|E|^2$) along the resonators for a TE_{10}/TE_{20} input mode mixture according to Fig. 18 at $f = 140$ GHz are plotted in Fig. 21.

V. CONCLUSION

Several compact single- (140 GHz) and two-frequency (105 and 140 GHz) notch filters with rectangular waveguide cross section have been designed, fabricated, and tested. The filters provide strong rejection of narrow frequency intervals both in F- and W-bands. This was realized by introducing symmetric steps in the width of standard WR08 and WR10 waveguides. Table I gives a comparison of the stopband widths at −30 and −60 dB with values of other filters built for application in plasma diagnostics. Due to the limited rejection of the coupled cavity filter described in [6], only the stopband width at −30 dB is given for this example. The filters described in [17], [18], and [19] are also based on cavities formed by extensions of the waveguide width. However, two-frequency notch filters, rejecting two distinct frequencies are, to our knowledge, for the first time described in this present article. In the case of

the WR10 waveguide filter, the second rejection frequency (140 GHz) is above the passband of the waveguide. In this case, the additional higher order mode (TE_{20}) is rejected. The measured notch depth for all filters is better than 80 dB at both 105 and 140 GHz.

ACKNOWLEDGMENT

REFERENCES

[1] V. O. Nichiporenko et al., "State of the art of 1 MW/105–140 GHz/10 sec gyrotron project in GYCOM," in *Proc. IRMMW-THz*, Shanghai, China, Sep. 2006, p. 338, doi: 10.1109/ICIMW.2006.368546.

[2] M. K. A. Thumm, G. G. Denisov, K. Sakamoto, and M. Q. Tran, "High-power gyrotrons for electron cyclotron heating and current drive," *Nucl. Fusion*, vol. 59, no. 7, Jul. 2019, Art. no. 073001, doi: 10.1088/1741-4326/ab2005.

[3] R. Ikeda et al., "Multi-frequency, MW-power triode gyrotron having a uniform directional beam," *J. Infr., Millim., THz Waves*, vol. 38, no. 5, pp. 531–537, May 2017, doi: 10.1007/s10762-016-0348-8.

[4] R. Marchesin et al., "Manufacturing and test of the 1 MW long-pulse 84/126 GHz dual-frequency gyrotron for TCV," in *Proc. IEEE Int. Vac. Electron. Conf. (IVEC)*, Busan, South Korea, Apr. 2019, pp. 1–2, doi: 10.1109/IVEC.2019.8745147.

[5] D. Wagner et al., "Status, operation, and extension of the ECRH system at ASDEX upgrade," *J. Infr., Millim., THz Waves*, vol. 37, no. 1, pp. 45–54, Jan. 2016, doi: 10.1007/s10762-015-0187-z.

[6] P. Woskov, "Notch filter options for ITER stray gyrotron radiation," in *Proc. 13th Int. Symp. Laser-Aided Plasma Diagnostics (NIFS-PROC)*, vol. 68, Gifu, Japan, 2007, pp. 38–41.

[7] M. Hirsch et al., "ECE diagnostic for the initial operation of Wendelstein 7-X," in *Proc. EPJ Web Conf.*, vol. 203, 2019, p. 3007, doi: 10.1051/epjconf/201920303007.

[8] J. W. Oosterbeek et al., "Assessment of ECH stray radiation levels at the W7-X Michelson interferometer and profile reflectometer," in *Proc. EPJ Web Conf.*, vol. 203, 2019, p. 3010, doi: 10.1051/epjconf/201920303010.

[9] D. Wagner et al., "Status of the new multi-frequency ECRH system for ASDEX upgrade," *Nucl. Fusion*, vol. 48, no. 5, May 2008, Art. no. 054006, doi: 10.1088/0029-5515/48/5/054006.

[10] G. I. Zaginaylov, V. I. Shcherbinin, K. Schuenemann, and M. K. Thumm, "Influence of background plasma on electromagnetic properties of 'cold' gyrotron cavity," *IEEE Trans. Plasma Sci.*, vol. 34, no. 3, pp. 512–517, Jun. 2006, doi: 10.1109/TPS.2006.875760.

[11] D. Wagner et al., "Bragg reflection band stop filter for ECE on Wega," *J. Infr., Millim. THz Waves*, vol. 32, no. 10, pp. 1424–1433, Dec. 2011, doi: 10.1007/s10762-011-9833-2.

[12] D. Wagner et al., "A multifrequency notch filter for millimeter wave plasma diagnostics based on photonic bandgaps in corrugated circular waveguides," in *Proc. EPJ Web Conf.*, vol. 87, 2015, p. 4012, doi: 10.1051/epjconf/20158704012.

[13] I. Arnedo et al., "Spurious removal in satellite output multiplexer power filters," in *Proc. EUMC*, Munich, Germany, 2007, pp. 67–70, doi: 10.1109/EUMC.2007.4405127.

[14] Q. Wang and J. Bornemann, "Synthesis and design of direct-coupled rectangular waveguide filters with arbitrary inverter sequence," in *Proc. ANTEM*, Jul. 2014, pp. 1–6, doi: 10.1109/ANTEM.2014.6887723.

[15] D. Wagner et al., "A compact two-frequency notch filter for millimeter wave plasma diagnostics," *J. Infr., Millim., THz Waves*, vol. 41, no. 7, pp. 741–749, Jul. 2020, doi: 10.1007/s10762-020-00701-6.

[16] D. Wagner, J. Pretterebner, and M. Thumm, "Transverse resonances in oversized waveguides," *Proc. SPIE*, vol. 2104, pp. 326–327, Aug. 1993.

[17] G. G. Denisov, S. V. Kuzikov, and D. A. Lukovnikov, "Simple millimeter wave notch filters based on rectangular waveguide extensions," *Int. J. Infr. Millim. Waves*, vol. 16, no. 7, pp. 1231–1238, Jul. 1995, doi: 10.1007/BF02068803.

[18] G. G. Denisov, A. A. Bogdashov, A. N. Panin, and Y. V. Rodin, "Design and test of new millimeter wave notch filter for plasma diagnostics," in *Proc. 33rd Int. Conf. Infr., Millim. THz Waves*, Pasadena, CA, USA, Sep. 2008, pp. 1–2, doi: 10.1109/ICIMW.2008.4665485.

[19] Y. Y. Danilov, G. G. Denisov, M. A. Khozin, A. Panin, and Y. Rodin, "Millimeter-wave tunable notch filter based on waveguide extension for plasma diagnostics," *IEEE Trans. Plasma Sci.*, vol. 42, no. 6, pp. 1685–1689, Jun. 2014, doi: 10.1109/TPS.2014.2318352.

[20] T. Lopetegi et al., "New microstrip 'wiggly-line' filters with spurious passband suppression," *IEEE Trans. Microw. Theory Techn.*, vol. 49, no. 9, pp. 1593–1598, Sep. 2001, doi: 10.1109/22.942571.

[21] C. Lechte, G. D. Conway, T. Görler, and C. Tröster-Schmid, "X mode Doppler reflectometry *k*-spectral measurements in ASDEX upgrade: Experiments and simulations," *Plasma Phys. Controlled Fusion*, vol. 59, no. 7, May 2017, Art. no. 075006, doi: 10.1088/1361-6587/aa6fe7.

[22] J. L. Doane, "Oversized rectangular waveguides with mode-free bends and twists for broadband applications," *Microw. J.*, vol. 32, no. 3, pp. 153–160, Mar. 1989.

Dietmar Wagner (Senior Member, IEEE) received the Dipl.-Ing. and Dr.-Ing. degrees in electrical engineering from the University of Stuttgart, Stuttgart, Germany, in 1990 and 1996, respectively.

He worked on high-power millimeter-wave transmission line components for the Ph.D. Dissertation and a Post-Doctoral Researcher at the Institute for Plasma Research, University of Stuttgart. From 1999 to 2001, he was with the Gyrotron Group, CPI Microwave Power Products Division, Palo Alto, CA, USA, where he worked on the design and development of high-power Gyrotron oscillators. In 2001, he joined the ECRH Group, Max Planck Institute for Plasma Physics, Garching, Germany, where he worked on the application of high-power millimeter waves for fusion plasma heating. Since 2011, he has been a Lecturer of high-power microwave technology at the Aix-Marseille Université, Marseille, France.

Walter Kasparek was born in Eitorf (Sieg), Germany, in 1952. He received the M.S. degree in physics and the Ph.D. degree in electrical engineering from the University of Stuttgart, Stuttgart, Germany, in 1979 and 1984, respectively.

In 1980, he joined the Institute for Plasma Research, University of Stuttgart, where he worked on co-laser scattering from coherent plasma density fluctuations. Since 1985, he has been working in the fields of plasma diagnostics with gyrotrons, electron cyclotron heating, and especially on high-power transmission and antenna systems for electron cyclotron heating and current drive in fusion experiments such as ASDEX Upgrade, Wendelstein 7-X, and ITER.

Fritz Leuterer, photograph and biography not available at the time of publication.

Francesco Monaco, photograph and biography not available at the time of publication.

Burkhard Plaum was born in Göttingen, Germany, in 1971. He received the Diploma and Ph.D. degrees in electrical engineering from the University of Stuttgart, Stuttgart, Germany, in 1997 and 2001, respectively.

He joined the Institute for Plasma Research, University of Stuttgart, where he worked on the design and optimization of oversized waveguide bends. Since then, he has been developing codes for the design of waveguide components, antennas, and mode converters; and analysis tools for experimental data.

Tobias Ruess received the B.S. degree in electrical engineering from the University of Ulm, Ulm, Germany, in 2015, and the M.S. degree in electrical engineering and information technology from the Karlsruhe Institute of Technology (KIT), Karlsruhe, Germany, in 2017.

He is currently with the Institute for Pulsed Power and Microwave Technology, KIT, where he is involved in the development of fusion gyrotron and measurement equipment.

Harald Schütz, photograph and biography not available at the time of publication.

Jörg Stober received the Dipl.-Phys. degree from ETH Zürich, Zürich, Switzerland, in 1988, and the Dr.rer.nat. degree from LMU Munich, Munich, Germany, in 1993.

He is the Leader of the ECRH Group for ASDEX Upgrade, Max Planck Institute for Plasma Physics, Garching, Germany. He is an ITER Science Network Fellow and is involved resolving final issues on design, commissioning, and safe operation of the ITER EC system. He is teaching plasma physics including nuclear fusion research at LMU Munich. His actual research interests include physics and operational limits of advanced tokamak scenarios.

Manfred Thumm (Life Fellow, IEEE) was born in Magdeburg, Germany. He received the Dipl.-Phys. and Dr.rer.nat. degrees in physics from the University of Tübingen, Tübingen, Germany, in 1972 and 1976, respectively.

At the University of Tübingen, he was involved in the investigation of spin-dependent nuclear forces in inelastic neutron scattering. From 1972 to 1975, he was Post-Doctoral Fellow with the Studienstiftung des deutschen Volkes, Dresden, Germany. In 1976, he joined the Institute for Plasma Research, Electrical Engineering Department, University of Stuttgart, Stuttgart, Germany, where he worked on RF production and RF heating of toroidal pinch plasmas for thermonuclear fusion research. From 1982 to 1990, his research activities were mainly devoted to electromagnetic theory and experimental verification in the areas of component development transmission of very high-power millimeter waves through oversized waveguides and of antenna structures for RF plasma heating with microwaves. In June 1990, he became a Full Professor at the Institute for Microwaves and Electronics, University of Karlsruhe, Karlsruhe, Germany, and the Head of the Gyrotron Development and Microwave Technology Division, Institute for Technical Physics, Research Center Karlsruhe (Forschungszentrum Karlsruhe: FZK). From April 1999 to September 2011, he was the Director of the Institute for Pulsed Power and Microwave Technology, FZK, where his current research projects have been the development of high-power gyrotrons, dielectric vacuum windows, transmission lines and antennas for nuclear fusion plasma heating, and industrial material processing. In October 2009, the University of Karlsruhe and the FZK have merged to the Karlsruhe Institute of Technology (KIT). He has authored/coauthored eight books, 21 book chapters, 620 research articles in refereed scientific journals, and around 1690 conference proceedings papers. He holds 14 patents on active and passive microwave devices.

Prof. Thumm was a member of the IEEE Nuclear and Plasma Sciences Society (NPSS) Plasma Science and Applications Committee (PSAC) Executive Committee and the IEEE EDS Vacuum Devices Technical Committee, and the Chapter MN6 Committee Vacuum Electronics and Displays of the Information Technical Society in German VDE (Chairperson from 1996 to 1999) and the German Physical Society. From 2007 to 2008, he was an EU member of the ITER Working Group on Heating and Current Drive, the Vice Chairperson of the Scientific-Technical Council of the FZK, and the Vice Chairman of the Founding Senate of the KIT. From 2008 to 2010, he was the Deputy Head of the Topic Fusion Technology of the KIT Energy. He was the General Chair of the Joint 29th International Conference on Infrared and Millimeter Waves and 12th International Conference on Terahertz Electronics (IRMMW 2004 / THz 2004) and IEEE 35th International Conference on Plasma Sciences (ICOPS 2008) in Karlsruhe, Germany. He has been a member of the International Organization and Advisory Committees of many international conferences and the editorial boards of several ISI refereed journals. From 2003 to 2010, he was the ombudsman for upholding good scientific practice at FZK/KIT. Since 2012, he has been an Editor for Vacuum Electron Devices of IEEE TRANSACTIONS ON ELECTRON DEVICES, a Distinguished Lecturer of IEEE NPSS, a KIT Distinguished Senior Fellow, and a member of the International Advisory Committee of Cooperative Innovation Center of THz Science in China. Since 2016, he has been serving as a member for the Scientific Advisory Council of the Leibniz Institute for Plasma Science and Technology Greifswald. Since 2020, he has been serving as a member for the International Steering Committee of the International Vacuum Electronic Sources Conference Series. He was awarded with the Kenneth John Button Medal and Prize 2000, in recognition of outstanding contributions to research on the physics of gyrotrons and their applications. In 2001, he was awarded the title of Honorary Doctor by the Peter the Great St. Petersburg Polytechnic University, for his outstanding contributions to the development and applications of vacuum electron devices. He received the IEEE-EDS 2008 IVEC Award for Excellence in Vacuum Electronics for outstanding achievements in the development of gyrotron oscillators, microwave mode converters and transmission line components, and their applications in thermonuclear fusion plasma heating and materials processing. Together with two of his colleagues, he received the 2006 Best Paper Award of the *Journal of Microwave Power and Electromagnetic Energy* and the 2009 CST University Publication Award. In 2010, he was awarded with the IEEE-NPSS Plasma Science and Applications Award for outstanding contributions to the development of high-power microwave sources (in particular gyrotrons) for application in magnetically confined fusion plasma devices as well as for stimulation and establishment of extensive international cooperations. He is a winner of the 2010 open grant competition of the Government of the Russian Federation to support scientific research projects implemented under supervision of Leading Scientists at Russian institutions of higher education (with Novosibirsk State University). Together with A. Litvak and K. Sakamoto, he was a recipient of the European Physical Society (EPS) Plasma Physics Innovation Prize 2011 for outstanding contributions to the realization of high-power gyrotrons for multimegawatt long-pulse electron cyclotron heating and current drive in magnetic confinement nuclear fusion plasma devices. In 2012, he was awarded with the Heinrich Hertz Prize of the EnBW Foundation and the KIT for outstanding contributions to generation, transmission, and mode conversion of high and very high microwave power for nuclear fusion and the HECTOR School Teaching Award in Embedded Systems Engineering. He received the Exceptional Service Award of the IRMMW-THz Society in 2017 and the IEEE NPSS Merit Award for his outstanding contributions and leadership in the field of electron cyclotron heating and current drive technology for thermonuclear fusion plasma research in 2018.